Determination of the Rate Constant for the NCO($X^2\Pi$) + O(^3P) Reaction at 292 K

Yide Gao and R. Glen Macdonald*

Chemistry Division, Argonne National Laboratory, 9700 South Cass Avenue, Argonne, Illinois 60439-4831

Received: October 18, 2002; In Final Form: March 6, 2003

The rate constant for the reaction of the isocyanate radical, NCO($X^2\Pi$), with oxygen atoms, O(^3P), has been measured at a temperature of 292 ± 2 K to be (2.1 ± 0.76) × 10^{-10} cm^3 molecule^{-1} s,$^{-1}$ where the error estimate contains both systematic and random errors. The measurements were carried out in an excess of either Ar or CF_4 at pressures between 1.5 and 7.5 Torr and found to be independent of both the nature of the third body and pressure. Equal concentrations of NCO and O were generated by the CN + O_2 reaction. The temporal dependence of NCO was followed using time-resolved infrared absorption spectroscopy on rotational transitions of the NCO (10^11) ← (00^10) combination band.

I. Introduction

There is an increasing effort to reduce the emission of NO_x compounds from combustion sources due to their detrimental effects on air quality. There are three established sources for NO_x formation in combustion: the Zeldovich or thermal NO_x mechanism, the Fenimore or prompt NO_x mechanism, and fuel-fixed nitrogen sources.[1] The latter two mechanisms are more kinetically complicated than the first, involving a large number of elementary reaction steps.[2] In both the prompt and fuel-fixed nitrogen mechanisms, CN and NCO radicals play key roles.

Many strategies have been proposed and implemented for NO_x abatement.[3] Neglecting catalytic conversion processes, these strategies involve the addition of various chemicals to the exhaust gas stream (selective noncatalytic reduction of NO, SNCR, processes) or the manipulation of the combustion process, including staged combustion and exhaust gas reburn techniques. The three main SNCR technologies are the following: the thermal De-NO_x process using NH_3 addition, the RAPRENO$_x$ process using $(HOCN)_3$ addition, and the NO_xOUT process using $(NH_2)_2CO$ addition. Again, the NCO radical plays an important role in the chemistry of these NO_x reduction technologies.[2,3]

In particular, one of the most important reactions involving the NCO radical and the conversion of N atoms into NO_x compounds is the reaction NCO + O because it directly converts a N atom into NO, and is also a chain termination step in the radical pool.[4] This reaction is important in both the chemistry of NO_x formation and its removal. There are three possible exothermic product channels:

$$\mathrm{NCO}(X^2\Pi) + \mathrm{O}(^3P) \rightarrow \mathrm{N}(^2D) + \mathrm{CO_2}(X^1\Sigma) \qquad \Delta H_f^0(0) = -68.6\ \mathrm{kJ\ mol^{-1}} \quad (1a)$$

$$\rightarrow \mathrm{N}(^4S) + \mathrm{CO_2}(X^1\Sigma) \qquad \Delta H_f^0(0) = -298.6\ \mathrm{kJ\ mol^{-1}} \quad (1b)$$

$$\rightarrow \mathrm{NO}(X^2\Pi) + \mathrm{CO}(X^1\Sigma) \qquad \Delta H_f^0(0) = -400.3\ \mathrm{kJ\ mol^{-1}} \quad (1c)$$

The $\Delta H_f^0(0)$ for NCO was taken to be 129.5 kJ mol^{-1}, as recommended by Smith.[5] A unique feature of all radical-atom reactions is the influence of multiple potential energy surfaces (PESs) on the reaction dynamics. For reaction 1, in C_s symmetry, the reactants correlate to three A′ and three A″ electronic PESs and doublet and quartet spin states, for a total of 12 PESs. If spin−orbit interaction is taken into account, there are 36 PESs correlating to the reactants.

There have been only a few measurements of the rate constant for reaction 1, k_1. The most recent measurements have been made by Becker et al.[6] These workers used UV laser photolysis to generate NCO from ClNCO and LIF to follow the time dependence of the NCO radical in a known concentration of O atoms. They reported k_1 measurements as a function of temperature from 297 to 757 K and found that k_1 exhibited a slight dependence on pressure near 300 K, increasing by a factor of about 2 for a pressure change from 2.5 to 9.9 Torr. The only other reported measurement of k_1 near 300 K has been from the early work of Schacke et al.[7] There have been several measurements of k_1 at high temperatures[8−11] and in flames.[12]

There have been no explicit theoretical studies of reaction 1; however, this reaction is closely related to the CN($^2\Sigma^+$) + O_2($^3\Sigma_g^-$) reaction, for which a detailed theoretical investigation of the saddle points and stationary points has been carried out on the reactive ^{2}A″ PES.[13] Thus, many features of the lowest-lying ^{2}A″ PES for the NCO + O system are known.

In the present work, k_1 was measured at 292 K in two carrier gases, Ar and CF_4, and as a function of pressure over a modest range from 1.5 to 7.5 Torr. Reaction 1 was initiated by photolyzing $(CN)_2$ at 193 nm to create CN radicals, which rapidly reacted with O_2 to produce equal concentrations of NCO and O.[14] The temporal dependence of the NCO radical was followed using time-resolved infrared absorption spectroscopy using several rotational transitions of the NCO(10^11) ← (00^10) combination band near 3.16 μm. The absorption coefficients for the monitored transitions have been previously determined,[15] so the absolute concentration of NCO was monitored. A chemical model was used to generate NCO concentration profiles to compare with experiment and determine k_1 by minimizing the sum of squares of the residuals between the experimental and calculated NCO concentration profiles. The

* To whom correspondence should be addressed. E-mail: rgmacdonald@anl.gov. Fax: (630) 252-9292.

10.1021/jp0222595 CCC: $25.00
Published on Web 05/15/2003

temporal dependence of the CN radical was also recorded to show consistency with the concentration of NCO.

II. Experimental Section

The experimental apparatus has been described previously, so only a brief description is given here.[16] The reaction vessel consisted of a rectangular stainless steel chamber containing a Teflon box with interior dimensions of 100 × 100 × 5 cm^3. The chamber could be evacuated to a pressure of 5.0×10^{-6} Torr with a diffusion pump and had a leak rate of about 5×10^{-4} Torr/min. Known flows of the reagent gases were admitted to the chamber from separate vacuum systems. Partial pressures were determined from the chamber pressure and known flow rates of the various gases. The total flow rate varied between 150 and 250 sccm. The gases used were Ar (AGA Gas, 99.995%), CF_4 (AGA Gas, 99.9%), O_2 (AGA Gas, 99.98%), and $(CN)_2$ (Spectra Gases, 98.0%). Generally, the gases were used as supplied by the manufacture except that the $(CN)_2$ was stored in a 20-L bulb and occasionally pumped on at liquid-nitrogen temperatures.

The photolysis laser was a Lamda-Physik Compex 205 excimer laser operating at a wavelength of 193 nm with an estimated fluence of 5−18 mJ cm^{-2} delivered to the photolysis region. To ensure that a fresh sample of gas was photolyzed on each laser pulse, the repetition rate was kept low, 1−3 Hz, with no detectable change in the rate constant measurements as a function of repetition rate.

The NCO($X^2\Pi$) radical was monitored using the $R_{1e/f}(12.5)$ or $P_{1e/f}(12.5)$ transitions of the $(10^01) \leftarrow (00^10)$ combination band centered near 3.16 μm. Time-resolved absorption profiles of NCO were obtained using the output of a Burleigh model 20 single-mode color center laser. The CN radical was also monitored using several rotational transitions of the CN "red system" ($A^2\Pi \leftarrow X^2\Sigma$) (2,0) band near 790 nm. Time-resolved absorption profiles of CN were obtained using the output of an Environmental Optical Sensor model 2010-EU tunable external-cavity diode laser. Both probe laser beams were spatially overlapped and multipassed through the photolysis region using a White cell. The photolysis laser was overlapped with the two probe laser beams by a UV−IR dichroic mirror positioned on the optical axis of the White cell.

The time-resolved absorption profiles for NCO and CN were recorded and signal-averaged using a LeCroy 9410 digital oscilloscope operating in the dc mode. The initial intensity, I_0, of the CN probe laser was obtained directly from the dc recorded signal. For the NCO probe laser, I_0 was measured using a box car triggered 100 μs before the excimer laser was fired. The infrared laser intensity before the White cell was held constant using an electrooptical feedback loop. For the small absorption signals observed in the infrared, a background signal due to thermal lensing and refractive index changes in the UV contacting optics was observed. This interference was removed from the signal by recording a background signal with the infrared laser tuned ~600 MHz from the line center and subtracting this background from the signal profile after transferring the data to a laboratory computer.

III. Results

A. Determination of Concentrations. In the present experiments, the probe laser bandwidth at frequency ν was much narrower than the line width of a Doppler-broadened spectral feature, so the laser frequency could be tuned to the peak absorbance of the probed transition and the temporal dependence of the transmitted laser intensity, $I(\nu)$, recorded. The Beer−Lambert Law relates the absorbance, $A(\nu)$, at time t to the concentration of species X, [X], according to[17]

$$A(\nu) = \ln(I_0(\nu)/I(\nu)) = l\sigma_{pk}(\nu)[X] \qquad (2)$$

where $I_0(\nu)$ and $I(\nu)$ are the incident and transmitted laser intensities, respectively, l is the path length, and $\sigma_{pk}(\nu)$ is the peak absorption cross section at ν. The experiments were carried out at sufficiently low pressure, 1.5−7.5 Torr, that the effect of pressure broadening should be small and the shape of an absorption feature should be well described by a Doppler line shape function. This enables $\sigma_{pk}(\nu)$ to be readily calculated if the line strength of the transition is known. The line strength for the NCO(10^01) ← NCO(00^10) $R_1(12.5)$ transition has been measured in this laboratory under conditions similar to those of the present experiment.[15] Unfortunately, the UV−IR dichroic optic has an absorption feature near 3.0 μm and improved signal-to-noise could be obtained if NCO was monitored further to the red of the $R_1(12.5)$ transition. Thus, the $P_1(12.5)$ transition was generally used to monitor the NCO concentration. The $R_1(12.5)$ line strength was converted to that for a $P_1(12.5)$ transition using the usual Hönl−London factor for a linear molecule and the dependence of the line strength on frequency. This procedure introduced a small uncertainty into the value of $\sigma_{pk}(\nu)$ due to the unknown ratios of the Herman−Wallis factors for these two transitions. The NCO rotational assignment required a detailed analysis of the NCO(10^01) ← NCO(00^10) transition, and a combination−difference analysis confirmed the rotational assignment.[18] Similarly, the line strengths for the CN($A\ ^2\Pi \leftarrow X\ ^2\Sigma$) (2,0) transitions used in the present work were taken from a theoretical calculation[19] and experimental measurement.[20] The $\sigma_{pk}(\nu)$ for NCO and CN used here are summarized in Table 1.

TABLE 1: The Peak Absorption Coefficient, $\sigma_{pk}(\nu)$, for the Transitions Probed in This Work Assuming a Doppler Line Shape for 292 K

molecule	transition	wavelength	$\sigma_{pk}(\nu)$ (cm^2 $molecule^{-1}$)
NCO	$(10^01) \leftarrow (00^10)$ $R_1(12.5)$	3.145 200 μm	$(3.7 \pm 0.4) \times 10^{-19}$ [a]
	$(10^01) \leftarrow (00^10)$ $P_1(12.5)$	3.165 073 μm	$(3.5 \pm 0.4) \times 10^{-19}$
CN	$(A^2\Pi \leftarrow X^2\Sigma)$ $R_1(14.5)$	790.029 nm	$(1.01 \pm 0.05) \times 10^{-16}$ [b]
	$(A^2\Pi \leftarrow X^2\Sigma)$ $R_1(4.5)$	789.995 nm	$(2.19 \pm 0.11) \times 10^{-16}$

[a] The uncertainty is one standard deviation, $\pm 1\sigma$, in the experimental determination. [b] The uncertainty is estimated from the theoretical calculation, ref 19, within the experimental determination, ref 20.

B. Mechanism and the Determination of the Rate Constant for NCO + O. Initially, the NCO radical and O atom were generated in equal concentrations by the reaction of CN + O_2. The CN radical was created by the 193 nm photodissociation of $(CN)_2$. Unfortunately, NO is produced in reaction 4b, and furthermore, NO + CO is expected to be the dominant product channel for the NCO + O reaction.[10] The reaction between NCO + NO is fast and competes with the NCO + O reaction for removal of NCO. The only other reaction involving the NCO radical is the possible reaction with $(CN)_2$. There is no available data on this reaction; however, the N−C bond is weak in NCO and the C−C bond is strong in $(CN)_2$, so a direct reaction is not possible. If the reaction proceeds by complex formation, the possible product channels could be CO + CN + NCN/CNN or N_2 + CO + CCN/CNC. However, all three channels are highly endothermic using the recent

TABLE 2: The Complete Chemical Model Describing the NCO + O Reaction System

no.	reactants		products	k (cm^3 molecule^{-1} s^{-1})	refs
1a	NCO + O	→	N(^{2}D) + CO_2	0.0[a]	
1b	NCO + O	→	N + CO_2	0.0[a]	
1c	NCO + O	→	NO + CO	*b*	this work
2	CN + CN + M[c]	→	$(CN)_2$ + M[c]	5.14×10^{-29} [d]	23
3	CN + O	→	CO + N	3.70×10^{-11}	24
4a	CN + O_2	→	NCO + O	1.87×10^{-11}	5, 14
4b	CN + O_2	→	NO + CO	5.41×10^{-12}	5, 14
4c	CN + O_2	→	N + CO_2	4.9×10^{-13}	5, 14
5	CN + NO + M[c]	→	CNNO + M[c]	1.64×10^{-30} [d]	25
6	NCO + N	→	N_2 + CO	5.5×10^{-11}	26
7a	NCO + NO	→	N_2 + CO_2	2.0×10^{-11}	27, 28
7b	NCO + NO	→	N_2O + CO	1.6×10^{-11}	27, 28
8	NCO + NCO	→	N_2 + 2CO[e]	5.0×10^{-12}	29
9	NCO + N_2O	→	N_2 + NO + CO[e]	5.7×10^{-14} [f]	30
10	NO + N	→	O + N_2	3.40×10^{-11}	31
11	first-order loss	→	diffusion	*g*	
12[h]	NO(v) + O_2	→	NO(0) + O_2	2.4×10^{-14}	32
13[h]	NO(v) + Ar or CF_4	→	NO(0) + Ar or CF_4	1.0×10^{-17}	33

[a] Products not determined. Channels 1a and 1b were assumed to be zero. [b] Varied. [c] M = Ar, CF_4, O_2. [d] Termolecular rate constant has units cm^6 molecule^{-2} s^{-1}. [e] The most likely products. [f] Currently under investigation. The k_9 is a current estimate. [g] Calculated from k_{diff}^{NO}. [h] Included to study the influence of NO(v) on reaction 7.

experimental measurements[21] of $\Delta H_f^{NCN} = 453$ kJ mol^{-1} and $\Delta H_f^{CNN} = 580$ kJ mol^{-1} and a theoretical estimate[22] of $\Delta H_f^{CCN} \approx \Delta H_f^{CNC} = 670$ kJ mol.$^{-1}$ Other rearrangements of these seven atoms seem unlikely. There are no other reactions involving the O atom except reaction 1 and loss by diffusion. Under these circumstances, it was felt that the best method for evaluating k_1 was to simulate the NCO temporal concentration profiles using a computer model of the chemistry occurring in the NCO + O system. The complete reaction mechanism,[14,23−33] consisting of 13 species and 10 reactions, is given in Table 2. For clarity, the most important reactions are

$$(CN)_2 \xrightarrow{193\ nm} 2CN(v,J)$$

$$CN + O_2 \rightarrow NCO(v_1,v_2,v_3) + O \quad (4a)$$

$$\rightarrow NO + CO \quad (4b)$$

$$\rightarrow N + CO_2 \quad (4c)$$

$$NCO + O \rightarrow NO + CO \quad (1c)$$

$$NCO + NO \rightarrow N_2 + CO_2 \quad (7a)$$

$$\rightarrow N_2O + CO \quad (7b)$$

$$NCO, O, NO \xrightarrow{k_{diff}} \quad (11)$$

The most significant reactions in the model, reactions 4 and 7, have been studied by several groups,[5,27,29,34,35] and their rate constants have been well established at 292 K. The first-order loss of each species from the photolysis region by diffusion, k_{diff}, could not be directly measured in the present experiments, but in another series of similar experiments, the loss of NO by diffusion was determined. For the other species, the first-order loss by diffusion was related to that for NO assuming k_{diff} was inversely proportional to the reduced mass for the species under consideration with respect to the average mass of the gas mixture.

As noted in the Introduction, the NCO + O reaction is closely related to the CN + O_2 reaction, and the products of reaction 1 are expected to be dominated by the more exothermic channel 1c, NO + CO. Attempts were made to monitor the NO product using the NO vibrational overtone (2) ← (0) $P_1(7.5)$ transition near 2.7 μm, but because of the small absorption cross section and low NO concentration created in these experiments, the signal-to-noise was insufficient to detect NO. The branching ratios for reaction 1 will have little effect on the determination of k_1 because the reactive products of reactions 1b and 1c, N and NO, respectively, react with NCO with similar rate constants, see Table 2. As will be discussed, the reaction path leading to channel 1a is expected to be much more constrained than that for channel 1c and, hence, not to compete with the much more exothermic channel 1c.

As noted above, NO produced in reactions 1c and 4b reacts with NCO; however, both of these reactions are sufficiently exothermic that a substantial amount of the reaction exothermicity could appear as vibrationally excited NO, NO(v). The influence of NO(v) on the determination of k_1 will be discussed in section III.C.

The rate equations describing the reaction mechanism in Table 2 were integrated using a fourth-order Runge−Kutta integration routine with variable step size,[36] and k_1 varied until the difference in the sum of the squares of the residuals, chi-squared, between the computer-generated and experimental NCO concentration temporal profiles was minimized. In the computer simulation of the NCO concentration temporal profile, the initial CN concentration, $[CN]_0$, was varied until the computer-calculated NCO concentration at a specified time, t, was within 1% of the experimentally observed NCO concentration at t. The specified time was chosen to occur at or slightly past the maximum in the experimental NCO concentration profile. The computer-generated $[CN]_0$ was compared to an experimental measurement of $[CN]_0$ to provide a consistency check on the NCO concentration. Because of the large discrepancy in their respective time scales, the CN radical was monitored in separate experiments from the NCO radical but under identical experimental conditions. However, the nonequilibrium internal energy distribution of the photolytically generated CN radicals and rapid reaction with O_2 made the experimental determination of $[CN]_0$ uncertain. These experimental measurements on CN will be discussed further in section III.E.

In an absorption experiment, the measured quantity is the degeneracy-weighted difference in populations between the quantum states connected by the radiative transition, so care must be exercised to ensure that the observed signal is indeed a true measure of the lower-state population, that is, the

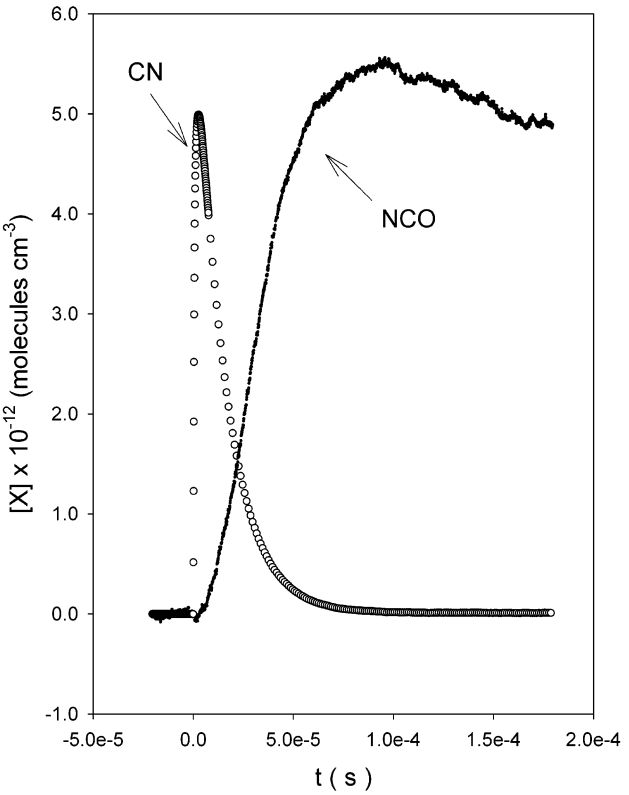

Figure 1. The initial temporal dependence of the concentration of CN(0) and NCO(00^10) measured simultaneously on the same photolysis laser pulse showing the rapid equilibration among the NCO vibrational manifolds. The measured absorbance profiles for each species were converted to population profiles using absorption coefficients assuming a temperature of 292 K and Doppler line widths. For the CN concentration profile, the data points are displayed every 10th point after 4 μs. The rates describing the CN concentration profile are $k_{rise} = 1.2 \times 10^6$ and $k_{decay} = 6.5 \times 10^4$ s^{-1} and those describing the NCO concentration profile are $k_{rise} = 1.6 \times 10^4$ and $k_{decay} = 5.9 \times 10^3$ s^{-1}. The conditions of the experiment were $P_{Ar} = 1.45$, $P_{O_2} = 0.109$, and $P_{(CN)_2} = 0.0775$ Torr.

upper-state population should be negligible. In Figure 1, the simultaneous removal of CN by reaction 4 and the production of NCO by reaction 4a are shown. Both profiles were recorded following the same photolysis laser pulse. The initial NCO(v_1,v_2,v_3) vibrational level distribution from reaction 4a has been studied by several different groups under both molecular beam[37] and bulb conditions.[38,39] The most notable observation is that under bulb conditions there is considerable excitation in the bending mode of NCO and only a small fraction of the reaction exothermicity appears in the stretching degrees of freedom. There have also been a number of investigations[40−42] on the vibrational relaxation of NCO, indicating that relaxation of the NCO(0,v_2^l,0) vibrational manifold is very rapid, even in collisions with inert gases. Furthermore, Sauder et al.[39] have measured the disappearance rates for many NCO vibrational levels with excitation in pure bend, stretch−bend, and combination stretch−bend manifolds. All of the relaxation measurements indicate that under the conditions of the present experiments, at a total pressure of 1.5−7.5 Torr, vibrational relaxation of NCO would occur on a time scale of a several tens of microseconds compared to the NCO + O reaction time scale of many milliseconds, so after a short induction time, the monitored NCO(00^10) vibrational level was in thermal equilibrium with the complete NCO vibrational manifold. Rapid vibrational relaxation of NCO(0,v_2^l,0) levels by inert gases is facilitated by the low bending fundamental, $\nu_2 = 532$ cm,$^{-1}$ and the Renner−Teller interaction.[43] These conclusions are borne out in Figure 1 in that the decay rate of CN is only a factor of 4 larger than the formation rate of NCO(00^10) and that the NCO(00^10) formation rate is in good agreement with the measured[41] vibrational rate constant for NCO(01^00) and NCO(01^20) → NCO(00^10) in collisions with Ar. At higher total pressures of Ar and CF_4 and higher partial pressures of O_2, the vibrational relaxation of NCO is even more rapid. In all of the experiments, the rate of the NCO(00^10) rise was only slightly smaller than the rate of loss of CN indicating that NCO vibrational equilibration was rapid and after a few tens of microseconds the measurement of the temporal dependence of NCO(00^10) concentration was a measure of the temporal dependence of NCO concentration.

The initial concentrations of NCO, $[NCO]_0$, and O, $[O]_0$, were varied by changing the photolysis laser power, keeping all other conditions the same. Typical NCO concentration temporal profiles are shown in Figure 2 in which the effects of varying the photolysis laser fluence from 6 to 15 mJ cm^{-2} are shown. The decay of NCO has a typical second-order appearance in which there is an initial rapid decay and a slow approach to the baseline. Note that the time to half-concentration becomes progressively shorter in going from panel a to panel d of Figure 2, as the initial radical and atom concentrations increase. The $[NCO]_0$ also increases linearly with the photolysis laser fluence with an intercept close to zero. The same behavior was found in both Ar and CF_4 carrier gases and a variety of O_2 partial pressures, clearly indicating that NCO was being removed by a second-order process.

The solid line in each panel of Figure 2 is the computer-generated NCO concentration temporal profile determined by varying k_1 to minimize the sum of the squares of the residuals between the experimental and computer-calculated NCO concentration profiles. Although the k_1 determined for each profile decreases with photolysis laser fluence, this is a coincidence for the chosen data set, and there is no correlation between k_1 and the photolysis laser fluence. Figure 2b is shown in more detail in Figure 3 to illustrate further the determination of k_1. In Figure 3, the open circles (○) are the experimental data points shown every 20 time intervals, and the solid line is the calculated NCO profile obtained by varying k_1 in the χ^2 minimization procedure. The two-dashed lines give the 95% confidence level in the determination of k_1. The insert in Figure 3 shows the χ^2 curve as a function of k_1. In the insert, the three large circles correspond to values of k_1 indicated in the legend. The rather large uncertainty in the evaluation of k_1 arises from the initial low concentration of the reacting transient species, NCO and O, and indicates that good signal-to-noise is needed to extract reliable rate constant data.

In dealing with a chemical mechanism involving many reactions, it is important to be able to identify the major reactions involved in the chemistry of any species in the reaction mechanism.[1] In the present work, this was accomplished by a reaction contribution factor, RCF, analysis.[1,2] For a reaction, I + J → products, with a rate constant k_{IJ}, the reaction contribution factor for species I reacting with species J at time t, RCF_J^I, is defined as the rate of reaction of I with J at time t, that is,

$$RCF_J^I = \frac{d[I]}{dt} = -k_{IJ}[J][I] \qquad (3)$$

where RCF_J^I, [J], and [I] are evaluated at time t in the reaction mechanism. The utility of the RCF is that the integral of RCF_J^I from $t = 0$ to time t gives the concentration of species I that

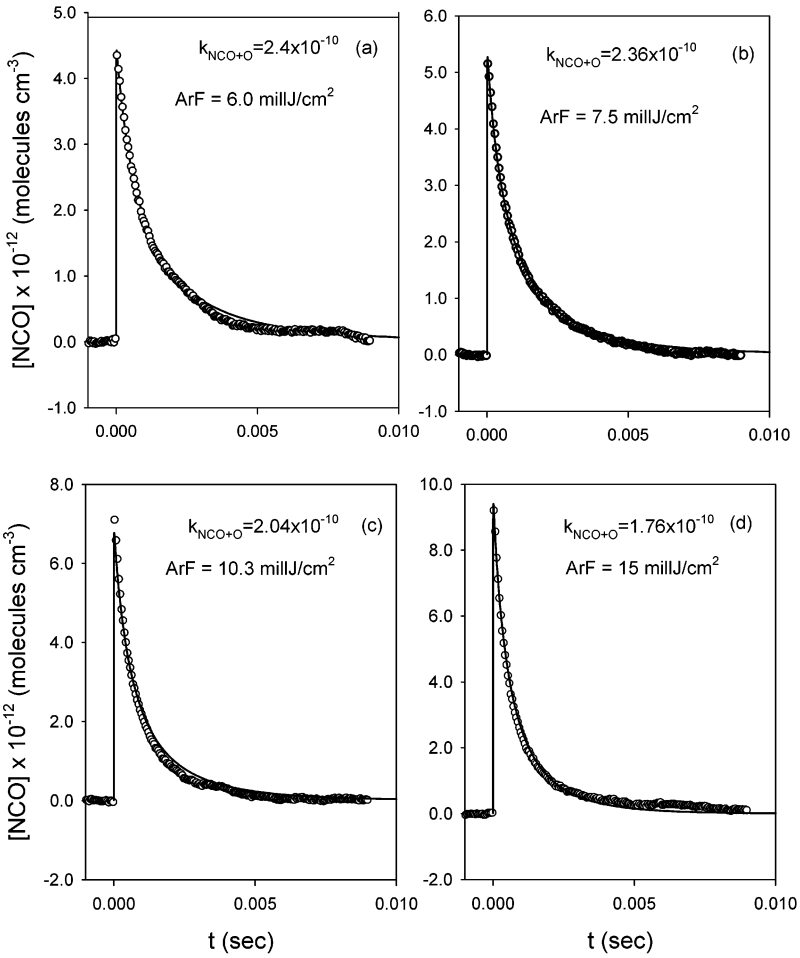

Figure 2. Typical experimental NCO concentration profiles and model calculations of NCO concentration for the value of k_1 that produced the best agreement between experiment and computer-calculated profiles as a function of photolysis laser fluence. The panels illustrate that the decay of NCO concentration is dominated by a second-order process; see text for a discussion. The conditions of the experiment were $P_{Ar} = 3.15$, $P_{O_2} = 0.423$, and $P_{(CN)_2} = 0.190$ Torr.

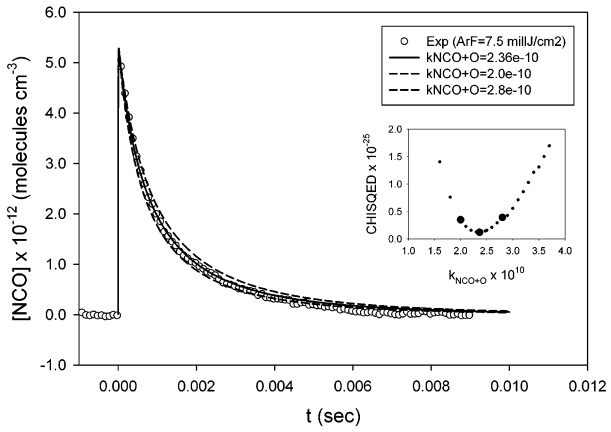

Figure 3. Figure 2b shown in more detail illustrating the range of k_1 values that describe the experimental NCO concentration profile. Every 20th experimental point is represented by the ○'s. The solid curve is the model NCO concentration profile that provided the best agreement with experiment for $k_1 = 2.4 \times 10^{-10}$ molecules cm^{-3} s.$^{-1}$ The smaller and larger values of k_1 provide estimates of k_1 at the 95% confidence interval, giving roughly a ±20% uncertainty in the determination of k_1. The insert shows χ^2 as a function of k_1.

was removed in reaction with species J up to time *t*. Thus the influence of species J on the concentration of I, either through k_{IJ} or the concentration of J, can be determined directly from the integrated RCF_J^I value. The RCF_X^{NCO} and integrated RCF_X^{NCO} for each species X that reacted with or produced NCO was calculated for each determination of k_1. The integrated RCF_O^{NCO}'s were found to vary between 0.4 and 0.8 depending on the conditions of the experiment, while that for the corresponding integrated RCF_{NO}^{NCO}'s were found to vary from 0.1 to 0.2. Removal by diffusion accounted for the other major pathway for loss of NCO. A plot of the RCF_X^{NCO}'s calculated in the computer simulation of the experiment illustrated in Figure 3 is shown in Figure 4. Note that reaction 1 accounts for 72% of the removal of NCO under the experimental conditions of Figure 3.

C. Influence of Vibrationally Excited NO. Oxygen atoms and NO are the only species that react with NCO to any significant extent. The rate constant, k_7, has been measured by several groups with good agreement. However, both reactions 1c and 4b are highly exothermic and could produce vibrationally excited NO, NO(v), which might react more rapidly with NCO than ground-state NO. Lin et al.[44] have examined the NCO + NO reaction using a theoretical description of the lowest singlet and triplet surfaces based on a BAC-MP4 calculation of the all of the stationary points and carried out detailed Rice−Ramsperger−Kassel−Marcus (RRKM) calculations for the rate constants and branching ratios. These theoretical calculations are in excellent agreement with all of the available experimental measurements on the NCO + NO system. Both product channels are produced through tight exit channel transition states with the result that as the temperature increases the initial OCNNO

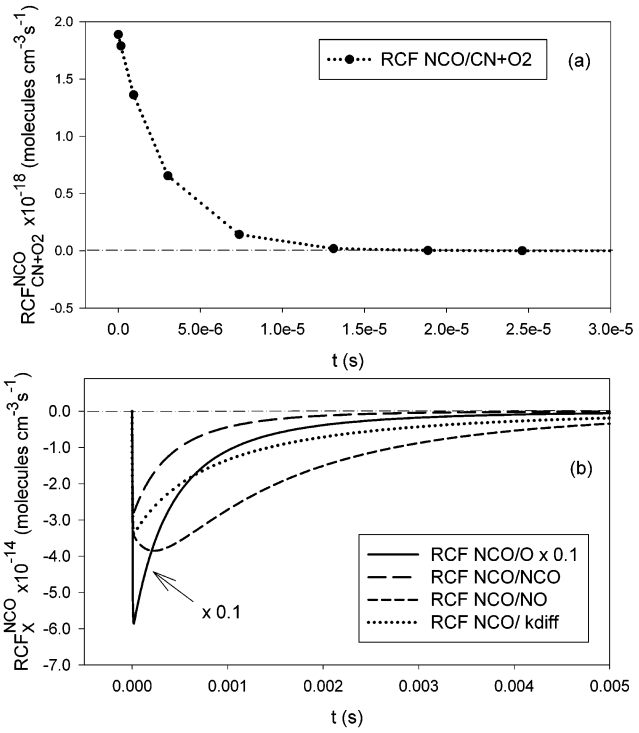

Figure 4. The (a) RCF^{NCO} for the production of NCO from the CN + O_2 reaction and the (b) RCF^{NCO}_X's for the removal of NCO by species with a final integrated RCF value greater than 1% of the NCO product. The computer calculation of the RCFs is for the determination of k_1 shown in Figure 3. Note that the RCF^{NCO}_O is a factor of 10 larger than any other RCF^{NCO}_X. The final integrated RCF^{NCO}_X's were 0.722, 0.0293, 0.160, and 0.0886 for reaction of NCO with O, NCO and NO and removal by diffusion, respectively.

adduct dissociates back to reactants rather than forward to products and the overall rate constant decreases. Furthermore, these entropic effects cause channel 7b to become dominant at higher temperatures. Under these circumstances, the influence of NO(v) would be expected to be similar to an increase in temperature and NO(v) would be expected to react with a smaller rate constant than NO(0). According to the RRKM theory of unimolecular reactions, the initial vibrational energy in NO would be rapidly randomized within the OCNNO adduct, thus favoring redissociation to reactants rather than passage through the tight transition states to products.

Although NO(v) should not react more rapidly with NCO than NO(0), several calculations were performed to explore the consequences of NO(v) on the determination of k_1. A worst-case scenario was adopted in that all of the NO produced in reactions 1c and 4b was assumed to be a single vibrationally excited species that reacted with NCO with a rate constant, k_7^v, and was relaxed by O_2 and Ar with the experimental[32,33] NO(1) vibrational relaxation rate constants. This value for k_{12} substantially under estimates the vibrational relaxation of NO(v) in the system because the vibrational relaxation of NO(v) by O_2 has been found[33] to increase by a factor of 20 for $v = 1-7$. Thus, the results of the simulations provide a lower bound for k_7^v. For the experimental run shown in Figure 3, the value found for k_7^v ranged from 5.7×10^{-11} for $k_1 = 2.4 \times 10^{-10}$ to 5.6×10^{-10} for $k_1 = 6.6 \times 10^{-11}$, in units of cm^3 molecules^{-1} s.$^{-1}$ Similar results were found for other simulations. It was concluded that for NO(v) to account for the observed NCO time dependence, the rate of k_7^v would need to be substantially larger than a hard sphere collision rate between NO and NCO, a highly unlikely situation.

TABLE 3: Summary of the Experimental Measurements for k_1 in Ar at 292 ± 2 K

P_{Ar} (Torr)	P_{O_2} (Torr)	$P_{(CN)_2}$ (Torr)	P_T (Torr)	$k_1 \times 10^{10}$ (cm^3 molecules^{-1} s^{-1})
1.32	0.0677	0.0812	1.47	1.44 ± 0.30^a
1.30	0.135	0.0808	1.51	1.52 ± 0.30
1.42	0.214	0.0734	1.70	1.92 ± 0.47
3.21	0.193	0.193	3.61	1.96 ± 0.069
3.19	0.298	0.192	3.69	1.87 ± 0.12
3.13	0.460	0.190	3.78	2.14 ± 0.30
4.76	0.169	0.170	5.10	2.45 ± 0.28
7.15	0.277	0.183	7.61	2.30 ± 0.46

Average of 27 Measurements:
$k_1 = (1.94 \pm 0.30) \times 10^{-10}$ (cm^3 molecule^{-1} s^{-1})

[a] $\pm 1\sigma$ from the average.

TABLE 4: Summary of the Measurements for the Determination of k_1 in CF_4 at 292 ± 2 K

P_{CF_4} (Torr)	P_{O_2} (Torr)	$P_{(CN)_2}$ (Torr)	P_T (Torr)	$k_1 \times 10^{10}$ (cm^3 molecules^{-1} s^{-1})
1.56	0.123	0.0657	1.75	2.06 ± 0.50^a
1.48	0.249	0.0682	1.80	1.97 ± 0.33
2.48	0.212	0.177	2.88	2.30 ± 0.28
2.25	0.501	0.160	2.91	2.51 ± 0.21
3.13	0.487	0.205	3.82	2.66 ± 0.47
3.89	0.306	0.205	4.40	2.91 ± 0.15

Average of 24 Measurements:
$k_1 = (2.37 \pm 0.34) \times 10^{-10}$ (cm^3 molecule^{-1} s^{-1})

[a] $\pm 1\sigma$ from the average.

D. Dependence on Third Body and Pressure. The results of previous work suggested that k_1 might exhibit a small pressure dependence.[6] To investigate this possibility, experiments were carried out over a modest pressure range and in the presence of a monatomic gas, Ar, and a polyatomic molecule, CF_4. CF_4 was chosen as a collision partner because polyatomic molecules are efficient at removing internal energy from highly excited molecules.[45] It also might enhance the vibrational relaxation of NO(v), which could interfere in the determination of k_1, as just discussed in the previous section. Furthermore, it is unlikely to react with CN and does not absorb at 193 nm. As noted previously, NO(0) could not be reliably detected in the present experiments, but other experiments in this laboratory indicated that CF_4 was about as efficient as Ar at vibrational relaxation of NO, so it did not prove to be an efficient quencher of NO(v). However, CF_4 was found to enhance the vibrational relaxation of NCO, as indicated by at least a factor of 2 increase in the rate of appearance of NCO(00^10) when Ar was replaced by CF_4.

The results for the determination of k_1 with Ar and CF_4 as carrier gas are summarized in Tables 3 and 4, respectively, and are presented in Figure 5. The measurements of k_1 were carried out over a pressure range of 1.3−7.2 Torr in Ar and 1.6−3.9 Torr in CF_4 with the partial pressure of O_2 varying between 0.07 and 0.5 Torr. The dependence of k_1 on O_2 was also investigated by varying the partial pressure of O_2, P_{O_2}, at a fixed total pressure. These results are displayed in Figure 5a. As can be seen from the figure, within the scatter of the measurements, the results are independent of P_{O_2}. This experiment is also a good indication that NO(v) had no effect on the determination of k_1 because $k_{12}P_{O_2}$ changed by almost an order of magnitude in these experiments and O_2 was the predominant collision partner for relaxation of NO(v).

From Figure 5b,c, it appears that k_1 increases as the pressure of the carrier gas increases; however, within the scatter in the measurements, indicated by the $\pm 1\sigma$ error bars, the measurements are independent of pressure. With Ar present, the value

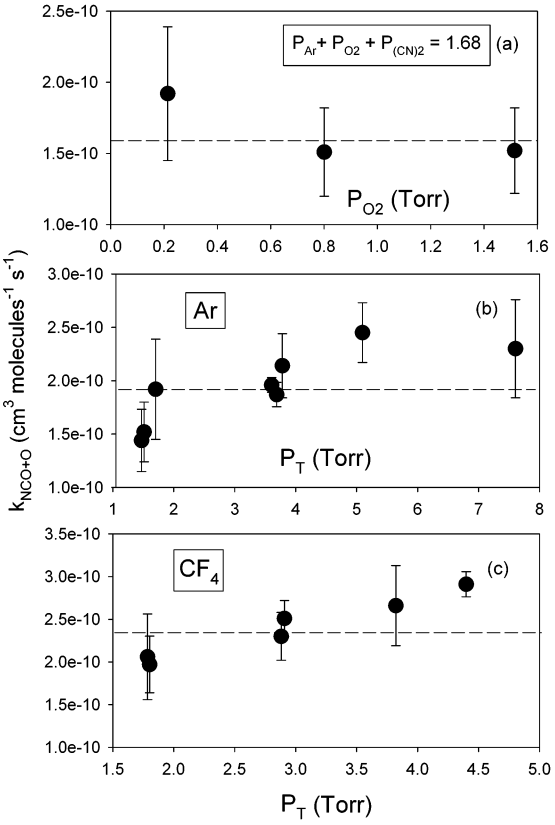

Figure 5. k_1 independence (a) from O_2 and likely NO(v), see text. The total pressure was constant at 1.68 Torr, and the P_{O_2} varied. Each data point is the average of 3−5 measurements of k_1 obtained by varying the ArF fluence, and the error bars are $\pm 1\sigma$ from the average. The dashed line is the average of the data weighted by the number of measurements. Panel b provides the summary of the data for the determination of k_1 with Ar as carrier gas. Each data point is the average of 3−5 measurements of k_1, as in panel a. The dashed line is the average of the data weighted by the number of measurements, giving $k_1 = (1.94 \pm 0.30) \times 10^{-10}$ cm^3 molecule^{-1} s.$^{-1}$ The data indicate that k_1 is independent of Ar pressure. Panel c provides the summary of the data for the determination of k_1 with CF_4 as the carrier gas. As in panel b, the average of the data weighted by the number of measurements of k_1 gives $k_1 = (2.37 \pm 0.34) \times 10^{-10}$ cm^3 molecule^{-1} s.$^{-1}$ The data indicate that k_1 is independent of CF_4 pressure.

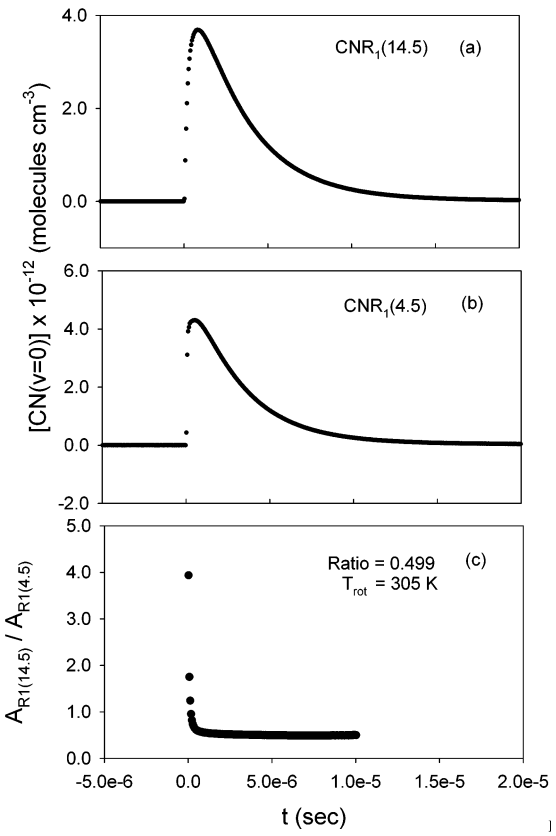

Figure 6. The temporal dependence of CN concentration determined (a) from monitoring the $R_1(14.5)$ transition and (b) from monitoring the $R_1(4.5)$ transition. The conditions of the experiment were $P_{Ar} = 3.15$, $P_{O_2} = 0.423$, and $P_{(CN)_2} = 0.190$ Torr. Panel c shows the ratio of the absorbance profiles used to calculate the CN concentration profiles in panels a and b. The first point corresponds to a rotational temperature of ∼1000 K, and the plateau region corresponds to a rotational temperature of 305 K. The temperature of the reaction vessel was 292 K.

of k_1 was determined to be $(1.94 \pm 0.30) \times 10^{-10}$ cm^3 molecule^{-1} s^{-1}, and with CF_4, the value of k_1 was found to be $(2.34 \pm 0.34) \times 10^{-10}$ cm^3 molecule^{-1} s^{-1}, both at a temperature of 292 ± 2 K. Within the scatter of these two measurements, the results are equal, and the average of these two measurements gives k_1 equal to $(2.14 \pm 0.31) \times 10^{-10}$ cm^3 molecule^{-1} s,$^{-1}$ independent of both pressure and the nature of the third body. The quoted uncertainty is $\pm 1\sigma$ from the average value.

E. Comparison of NCO Concentration and CN Concentration. As discussed in section III.A, the temporal dependences of both NCO concentration and concentration of CN radicals were monitored under the same experimental conditions. As noted previously, the determination of CN concentration was intended to serve as a consistency check on the measured NCO concentration. This is important because the value of k_1 depends on the absolute concentration of NCO. In addition, two rotational transitions of CN were monitored to provide an estimate of the temperature in the photolysis region. The temporal dependence of CN concentration calculated from the absorbance profiles for the CN($A^2\Pi \leftarrow X^2\Sigma$) (2−0) $R_1(14.5)$ and $R_1(4.5)$ transitions for the same experimental run as in Figure 3 is shown in Figure 6a,b. A plot of the ratio of these two absorbance profiles is shown in Figure 6c. From this ratio and the CN $R_1(J)$ line strengths, an estimate of the rotational temperature describing the population in the two levels can be made. Following an initial transient, the ratio of these absorbances reaches a plateau corresponding to a rotational temperature of 305 K.

Generally, the CN rotational temperature varied between 300 and 330 K. The reason for the difference between the measured rotational temperature and the temperature of the reaction vessel is not known. An estimate of the temperature rise from the absorbed photolysis energy can be made. Using the 193 nm absorption coefficient[46] for $(CN)_2$ (1.1×10^{-19} cm^2 molecule^{-1}) and a $P_{(CN)_2}$ of 0.2 Torr, the maximum used in the experiments, we calculated the attenuation of the photolysis laser intensity to be 10% over the 140 cm long photolysis zone, giving a maximum temperature rise of 1 K from the initial photodissociation step and the energy released in reaction 1. A further temperature rise of 5 K was estimated from the subsequent NCO + O chemistry, according to the calculated integrated RCF factors for the various reactions. Although care was taken to ensure that the CN probe laser frequency was tuned to the peak in the Doppler profile, uncertainty in this step would tend to favor a higher rotational temperature especially because the CN absorbances were large, varying between 1 and 2.5 for the lower J transition. The 193 nm photolysis of $(CN)_2$ produces an initial rotational state distribution[47] that has considerable rotational excitation, with the peak of the J distribution around $J = 25.5$ and a rotational temperature of approximately 2200 K. It is

possible that quenching of rotational levels with large J values contributes to the population into the lower levels at a rate slower than the expected rotational relaxation rate for low J states among themselves, giving rise to an apparently higher rotational temperature, that is, an excess of population in the monitored rotational state having the larger J value.

As discussed in section III.B., in the model simulations, $[CN]_0$ was varied until the model $[NCO]_t$ agreed within 1% with the experimentally observed $[NCO]_t$ value; thus, the simulations returned a value of $[CN]_0$ that can be compared to the experimental measurement. However, there is some uncertainty as to the best way to evaluate $[CN]_0$ from the experimental profiles shown in Figure 6a,b. Using a nonlinear least-squares analysis, the CN concentration temporal profiles were fit to the sum of two decaying exponential terms, having negative and positive preexponential factors. A zero-order interpretation of these terms is that the negative preexponential term describes the formation of CN(J) from rotational relaxation of excited rotational levels,[47] k_{rise}, and the positive preexponential decay describes the reaction of CN(J) with O_2, k_{decay}. In a simple two-step model, given by $[CN]_0 \rightarrow [CN(J)] + O_2 \rightarrow$ products, the coefficient of the positive exponential term is simply $[CN]_0$ if $k_{rise} \gg k_{decay}$. This suggests that the coefficient of the positive exponential term should be identified with $[CN]_0$. However, there is some uncertainty in the determination of this preexponential factor because of the rapidly changing absorbance in the first few microseconds of the CN profile, as shown in Figure 6. In this transient time interval, indicated by the rapid change in the absorbance ratio in Figure 6c, not only is the rate constant for reaction k_4 changing and approaching its room temperature value, but simultaneously both translational and rotational relaxation are occurring. The influence of these transient events on the determination of the preexponential factor for the k_{decay} term is not easy to determine. Alternately, the decay could be fit to a single-exponential term starting at sometime after this transient interval has passed. However, in this case the determination of the starting time for the extrapolation and, also, the correct $t = 0$ are ambiguous, again because of the transients just noted. The determination of $[CN]_0$ by both methods gave similar results with the single exponential fit method giving consistently larger values (5%−10%). The two exponential term method was adopted here because of its more unbiased implementation. With increasingly larger values of $k_{decay} = k_4 P_{O_2}$, the transient region becomes a larger fraction of the complete CN decay interval, and as a result, the experimental determination of $[CN]_0$ becomes more uncertain.

Although the intent of monitoring CN was to compare the measured $[CN]_0$ to the value predicted in the model calculations and, hence, to provide a check on the measured NCO concentration, it also provided an estimate of k_4, assuming $k_{decay} = k_4 P_{O_2}$. Indeed, the integrated RCF^{CN} analysis indicated that under all conditions reaction 4 accounted for more than 99% of the removal processes for CN. With Ar and CF_4 as carrier gas, k_4 was found to be $(2.31 \pm 0.12) \times 10^{-11}$ [35] and $(1.95 \pm 0.15) \times 10^{-11}$ [20] cm^3 molecule^{-1} s^{-1}, respectively, at a temperature of 292 ± 1 K, where the numbers in brackets indicate the number of measurements. Reaction 4 has been measured in several laboratories,[5] and a value of $(2.42 \pm 0.19) \times 10^{-11}$ cm^3 molecule^{-1} s^{-1} has been recommended for 292 K. The value for k_4 determined in Ar as the carrier gas is in good agreement with the recommended value; however, that measured in CF_4 is not. The reason for this discrepancy is not quite clear, but on average, the P_{O_2} was higher in the CF_4 experiments, and the initial transient region likely had more influence on the measurement of k_4 in the CF_4 experiments.

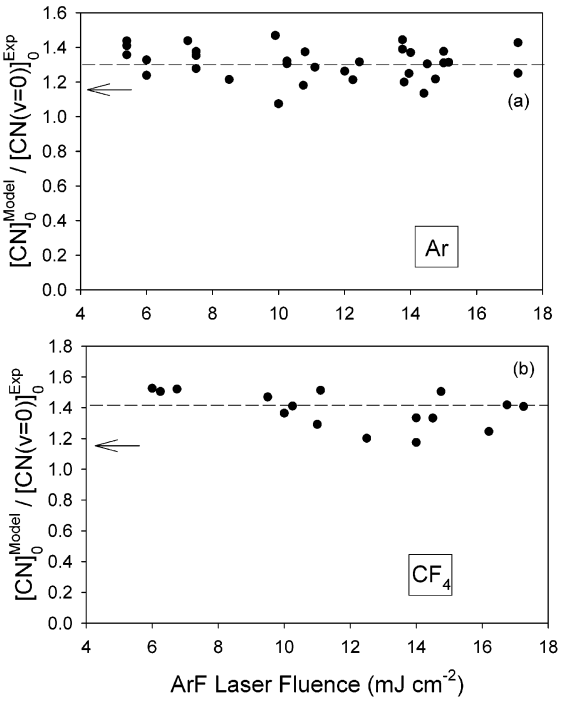

Figure 7. The $[CN]_0^{model}/[CN(v=0)]_0^{exp}$ is shown as a function of photolysis laser fluence (a) with Ar as the carrier gas and (b) with CF_4 as the carrier gas. The average of all the experiments is shown by the dashed line. The arrow indicates the most recent experimental measurement.[47] The results indicate that within the scatter of the measurements the NCO concentration was determined accurately.

Only the ground vibrational state of CN could be monitored in the present experiments; however, vibrationally excited CN(v=1, 2) can also be produced in the 193 nm photolysis of $(CN)_2$. The most recent CN vibrational state distribution determined[47] by North and Hall is 0.87 ± 0.02, 0.13 ± 0.02, and 0.003 ± 0.001 for v = 0, 1, and 2, respectively. The ratios of $[CN]_0^{model}/[CN(v=0]_0^{exp}$, where $[CN]_0^{model}$ was calculated in the computer simulations described in section III.B, and $[CN(v=0)]_0^{exp}$ was determined using the preexponential factor of the k_{decay} exponential term, are shown in Figure 7, part a for Ar and part b for CF_4, and the average values of $[CN]_0^{model}/[CN(v=0)]_0^{exp}$ were found to be 1.31 ± 0.10 and 1.39 ± 0.12 in Ar and CF_4 carrier gases, respectively. When the CN vibrational distribution measured[47] by North and Hall is used, the predicted value should be 1.15 ± 0.04. The agreement between the model predictions of the $[CN]_0$ and the experimental values is not perfect, but on the other hand, they are in agreement within the experimental uncertainty by $\pm 1\sigma$ for Ar and $\pm 2\sigma$ for CF_4. The experimental determination of $[CN]_0$ presented in Figure 7 indicates that the $[CN]_0$ needed to reproduce the NCO concentration used in the computer simulations of the NCO concentration profiles was within 15%−25% of the measured value. This is taken as an independent confirmation that the NCO concentration determination was correct at least within the experimental uncertainty in the measured NCO peak absorption coefficient, Table 1.

IV. Discussion

A. Error Analysis. There are several sources of error contributing to the uncertainty in the determination of k_1. The first is the determination of the absolute concentration of the

TABLE 5: Summary of the Average Fractional Uncertainty in the Fitted k_1 and the Average Fractional Removal of NCO by O and NO

carrier gas	avg $\pm\Delta k_1/k_1$	SD	avg $\int RCF_O^{NCO}$/total	SD	avg $\int RCF_{NO}^{NCO}$/total	SD
Ar	0.15	0.09	0.66	0.14	0.15	0.035
CF_4	0.14	0.09	0.72	0.07	0.11	0.015

NCO radical. The details of the experiment carried out to measure the $\sigma_{pk}(\nu)$ for the NCO transitions used in this work will be presented elsewhere;[15] however, the experimental uncertainties in these measurements have been summarized in Table 1. Two other effects related to the spectroscopy of NCO that could influence the determination of the NCO concentration are the Herman−Wallis effect and pressure broadening. Both effects are presumed to be small under the present experimental conditions. In molecules similar to NCO, NO, CO_2, and N_2O, the Herman−Wallis effect contributes less than 2% to the line strength for similar transitions.[48,49] With increasing pressure, pressure broadening causes a reduction in $\sigma_{pk}(\nu)$ from the Doppler value and would result in an underestimation of the NCO concentration, eq 2 and, hence, an overestimation of k_1. Indeed, the trend in k_1 as a function of pressure for both Ar and CF_4, parts b and c of Figure 5, respectively, appears to be in agreement with this prediction; however, the scatter in the measurements is sufficient to obscure such behavior. The uncertainty in the determination of $\sigma_{pk}(\nu)$ of $\pm1\sigma$ results in an uncertainty in the determination of k_1 of $\mp1\sigma$. Note that the uncertainty in the determination of NCO concentration does not introduce any further uncertainty into the O concentration because of the initial stoichiometric relationship between the $[NCO]_0$ and $[O]_0$ initiated in reaction 4a.

The other factors influencing the uncertainty in the determination of k_1 are the goodness-of-fit for the computer-generated NCO concentration profiles to the experimental ones, and the uncertainty in the rate constants used in the model simulations. Fortunately, the kinetic scheme given in Table 2 is relatively simple, and there are only three major processes contributing to the removal of NCO, reactions 1 and 7 and diffusion. As already discussed in section III.C, the NCO radical could react more rapidly with NO(v); however, it was argued there that this possibility was unlikely. The computer program used to determine k_1 provided an estimate of the goodness-of-fit for k_1 (see the insert in Figure 3) and an RCF analysis, as discussed in section III.B. As noted there, the integrated RCF_J^{NCO}'s provided a direct means of measuring the removal of NCO by reaction with species J or removal by diffusion. For each experiment, the fractional uncertainty in the fitted k_1 and the fractional contribution for the removal of NCO by O, NO, and diffusion were tabulated. The average values and the standard deviation in these quantities are listed in Table 5. From this table, it can be seen that on average the value of k_1 that was found to best describe the NCO concentration temporal profile was determined to within $\pm15\%$ at the 68% confidence level. Note that this average uncertainty is the same as the standard deviation in the scatter of the measurements for k_1, Tables 3 and 4, which it should be if there are no other large sources of random error.

As is shown in Table 5, the average contribution of reaction 7 to the total NCO removal was 15% with Ar and 11% with CF_4 as carrier gas. Reaction 7 has been investigated by numerous workers,[27,29,34,35] and the average value for k_7 is $(3.6 \pm 0.5) \times 10^{-11}$ cm^3 molecule^{-1} s^{-1}, where the uncertainty is $\pm1\sigma$. Thus, on average, the 15% uncertainty in the literature value for k_7 contributes $\mp2\%$ uncertainty to the determination of k_1. Similar considerations apply to the loss of species by diffusion. The average removal rate by diffusion contributed 10% to the total removal of NCO. The uncertainty in the diffusion rate was estimated to be $\pm20\%$, so the diffusion process also contributed a $\mp2\%$ uncertainty to the determination of k_1.

The total uncertainty in the determination of k_1 can be summarized as follows: spectroscopic,15%; random scatter in the determination of k_1, 15%; uncertainty in the rate constants directly influencing the determination of k_1, 4%; determination of partial pressures, 2%. Combining the measurements of k_1 for the two carrier gases gives k_1 equal to $(2.1 \pm 0.76) \times 10^{-10}$ cm^3 molecule^{-1} s,$^{-1}$ at 292 K, independent of carrier gas and pressure, where the quoted uncertainty reflects both systematic and random errors.

B. Comparison with Previous Work. The available data[6−12] for k_1 is shown in Figure 8 as a function of temperature. As is evident from the figure, the determination of k_1 in the present work is substantially larger than previous measurements near 300 K, although the results do just overlap those of Becker et al.[6] if the absolute error bars are extended to the $\pm2\sigma$ level of uncertainty. Furthermore, the previous suggestion[6] that k_1 exhibited a slight pressure dependence was not borne out in the current work. Within the scatter of the measurements, k_1 was found to be independent of both the nature of the third body collision partner and pressure, as shown in Figure 5 and Tables 3 and 4.

As is evident from Figure 8, the low-temperature measurement of k_1 found in this work and the high-temperature data show that k_1 exhibits a negative temperature dependence. A nonlinear least-squares fit to the value of k_1 measured in this work and the high-temperature measurements from Prof. Hanson's laboratory[10,11] gives k_1 equal to $1.96 \times 10^{-10}(300/T)^{0.50}$ cm^3 molecule^{-1} s.$^{-1}$ This fit is illustrated by the dotted curve in Figure 8. Interestingly, the temperature dependence of the rate constant for the related reaction, CN + O_2, also exhibits a similar $T^{-0.5}$ dependence.[5] Reactions 1 and 4 can occur on the same global CNOO PES but of course sample different regions. The CN + O_2 reaction leading to the NCO + O products occurs through the C and O atom interaction, while the NCO + O atom reaction is likely dominated by the N and O atom interaction. Mohammad et al.[50] have suggested that the CN + O_2 reaction channel leading to NO + CO products arises from an exit channel interaction in which the rotational motion of the departing NCO and O fragments results in a secondary encounter between the N and O atom leading to the NO + CO products. The large value for k_1 measured in the present work indicates that the chemical forces between the O atom and N atom of NCO are strong and supports the interesting conjecture of Mohammad et al.

There are several other important observations on the NCO + O reaction system. Approximating the collision diameter of NCO to that of CO_2, we estimate a hard-sphere collision rate between NCO and O to be 1.8×10^{-10} cm^3 molecule^{-1} s^{-1} at 292 K. Thus, every encounter between NCO and O within their hard-sphere collision radius leads to reaction. These collisions can occur on multiple PESs, involving both the electronic and spin manifolds. Assuming C_s symmetry and neglecting spin−orbit interactions, on the reactant side, NCO($^2\Pi$) and O(^3P_g) correlate with $3(^{4,2}A' + {}^{4,2}A'')$ PESs, while on the product side, the following correlations exist: the $N(^2D_u) + CO_2(^1\Sigma^+)$ product channel correlates to $3(^2A'') + 2(^2A')$; the $N(^4S_u) + CO_2(^1\Sigma^+)$ channel correlates to $^4A''$; the $NO(^2\Pi) + CO(^1\Sigma^+)$ channel correlates to $^2A'' + {}^2A'$. (Note that the $CN(^2\Sigma^+) + O_2(^3\Sigma_u^-)$ reaction correlates to $^{4,2}A''$ PESs.) Of course, in general C_1

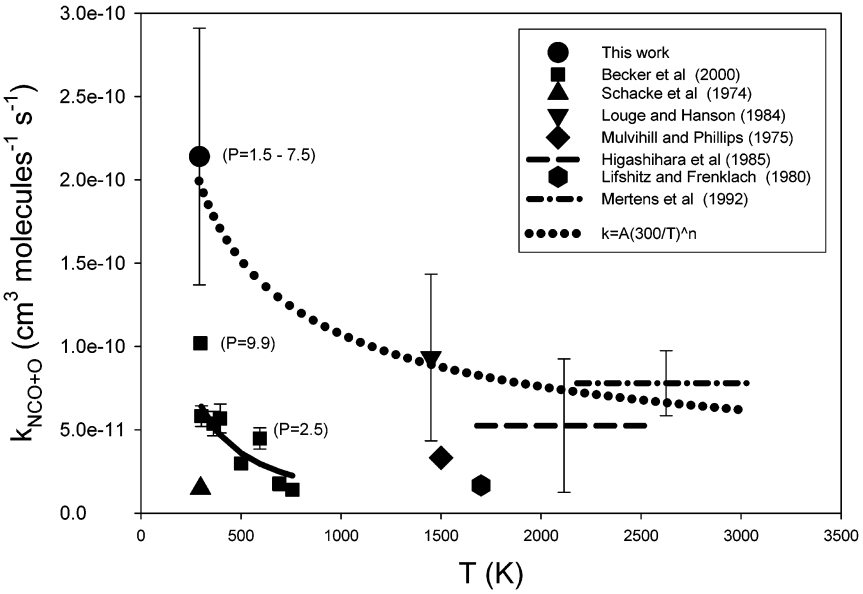

Figure 8. The temperature dependence for k_1. The error bars indicate an estimate of the absolute errors in the experiment, except for the work of Becker et al.[6] in which they indicate the scatter in the measurements. The dotted line is a fit of the room-temperature measurement of this work, Louge and Hanson,[10] and Mertens et al.[11] of the form $k_1 = A(300/T)^n$, where $A = 1.96 \times 10^{-10}$ and $n = 0.50$. The various measurements are (●) this work, (■) Becker et al.,[6] (▲) Schacke et al.,[7] (▼) Louge and Hanson,[10] (◆) Mulvihill and Phillips,[12] (− − −) Higashihara et al.,[9] (⬢) Lifshitz and Frenklach,[8] and (− · −) Mertens et al.[11]

symmetry, the A′ and A″ symmetry labels are lost, but at least, conceptually, it is easier to view the collision confined to a plane.

There have been no theoretical calculations undertaken to explore the initial interaction between NCO and O; however, simple electronic orbital considerations can provide some insight. The most attractive interaction should occur on a ^{2}A″ PES described by a bonding interaction between one of the singly occupied p-orbitals on the O atom approaching the singly occupied p-orbital on the N atom, lying in the plane of the four atoms. If the singly occupied N atom p-orbital is perpendicular to the four atom plane, the PES is of ^{2}A′ symmetry and should be more repulsive because of electron−electron repulsion between the in-plane singly occupied O atom p-orbital and the now in-plane bonding N−C p-orbitals. On the lowest-lying ^{2}A″ PES, the interaction should proceed with little or no barrier because there is nothing to impede the direct formation of a chemical bond between the N and O atoms. This PES is likely the same ^{2}A″ PES on which the CN + O_2 reaction occurs and has been described recently by Qu et al.[13] at the B3LYP level of theory for geometries and the CCSD(T) level of theory for energies. Their Figure 3 can be used to extend the reaction sequence on this most attractive ^{2}A″ PES. (In the following, the designations of Qu et al.[13] for transition states and stationary points will be used and indicated by **bold** type.) The initial attractive interaction between the O and N atom should lead directly to the most deeply bound intermediate on the ^{2}A″ PES, structure **3**, having a zigzag OCNO arrangement of atoms. A small barrier of 14 kJ mol^{-1} through transition state **TS3/B** leads directly to the NO + CO product channel (**B**). Other reaction paths leading from adducts formed by the O atom approaching the O end of NCO, structures **1** and **6**, can also be formed without barriers but connect to the NO + CO product channel over transition states that lie above the NCO + O energy asymptote and do not contribute to reaction at low temperatures.

Another possible channel for the NCO + O reaction on the ^{2}A″ PES is the N(^{2}D) + CO_2 channel. Again referring to Figure 3 of Qu et al.,[13] the O atom can approach the central C atom of NCO without a barrier to form adduct **6**, having a C_{2v} N−COO structure. This adduct can dissociate back to the NCO + O reactants or to the N(^{2}D) + CO_2 channel, which was calculated to be 30 kJ mol^{-1} (69 kJ mol^{-1} thermodynadically) lower in energy. The competition between these two processes will depend critically on the exact nature of the reaction path taken in each case. It is expected that the reaction path leading to the formation of adduct **6** (the formation of the N(^{2}D) + CO_2 channel) would be significantly more constrained than the one along the path leading to the more exothermic NO + CO channel, and the latter should be strongly favored. The product channels for reaction 1 have not been determined experimentally or examined theoretically; however, channel 1c is expected to dominate. Nevertheless, if channel 1a is significant, the reaction of N(^{2}D) with O_2 would generate NO(v) + O and could lead to an over estimation of k_1 because of the increased O and NO concentrations.

The theoretical calculations of Qu et al.[13] dealing with the CN + O_2 ^{4}A″ PES indicate that the interaction between CN and O_2 is mostly repulsive. This is in agreement with other work.[51] There are no theoretical descriptions for the interaction between NCO and O on the global CNOO ^{4}A″ PES, and it is assumed that the interaction will likely be repulsive or at least not as attractive as the ^{2}A″ PES.

There are still 10 other PESs within both the doublet and quartet spin manifolds. Statistically, the collisions between NCO and O should occur equally within the A″ and A′ electronic manifolds with $^2/_3$ of the collisions occurring within the quartet spin manifold; however, k_1 is approximately the hard-sphere collision rate at 292 K. Clearly, intersystem crossing and internal conversion must be facile in this system if the experimental measurement reported on here is correct. There must be some mechanism to promote these processes. There are two possibilities. The formation of long-lived adducts could allow the crossing seams between electronic and spin manifolds to be sampled multiple times.[52,53] Alternately, these transitions could occur at long range where the separations between the various PESs are small and the newly forming spin quantum has not been fully developed. In any case, detailed theoretical investiga-

tions of the influence of multiple PESs will be needed to address this issue for the NCO + O system and other radical−radical systems.[54,55]

It has recently been shown[56] that the large reaction exothermicity available in many radical−radical reactions can lead to new dynamical features influencing product branching ratios. Product channels can be produced without a transformation through a localized transition-state configuration, and this direct dynamics mechanism can be responsible for a large number of reactive trajectories. Detailed theoretical calculations will be necessary to determine whether this direct dynamics mechanism also occurs in the NCO + O system.

V. Conclusion

The rate constant for the NCO($X^2\Pi$) + O(^3P) reaction has been measured to be $(2.1 \pm 0.76) \times 10^{-10}$ cm^3 molecule^{-1} s^{-1} at a temperature of 292 ± 2 K, where the error bars account for both random and systematic error. The rate constant was found to be independent of both pressure over the pressure range of 1.5−7.6 Torr and the nature of a third-body collision partner. The measured k_1 is slightly larger than an estimate of the hard-sphere collision rate constant between NCO and O and indicates that intersystem crossing and internal conversion must be facile in this system. The expected dominant product channel 1c, NO + CO, correlates with the doublet manifold; however, adiabatically, $^2/_3$ of the collisions initially start out in the quartet-spin manifold. The identification of the product channels for this reaction would confirm the speculation of the importance of nonadiabatic effects in simple radical−radical reactions. Further theoretical work on the nature of the complete $3(^{4,2}A'' + ^{4,2}A')$ system of PESs would also be very useful.

The result of this work was combined with high-temperature shock tube measurements to determine the temperature dependence of k_1 to be $(1.9(300/T)^{0.50}) \times 10^{-10}$ cm^3 molecule^{-1} s^{-1}. The NCO + O rate constant appears to have the same general temperature dependence as the CN + O_2 reaction, that is, $T^{-0.5}$.

Acknowledgment. This work was supported by the U.S. Department of Energy, Office of Basic Energy Sciences, Division of Chemical Sciences, Geosciences, and Biosciences, under Contract No. W-31-109-ENG-38.

References and Notes

(1) Warnatz, J.; Maas, U.; Dibble, R. W. *Combustion: Physical and Chemical Fundamentals, Modeling and Simulation, Experiments, Pollution Formation*; Springer: Berlin, 1995.
(2) Miller, J. A.; Bowman, C. T. *Prog. Energy Combust. Sci*. **1989**, *15*, 287.
(3) Bowman, C. T. In *Pollutants from Combustion*; Vovelle, C., Ed.; Kluwer Academic Publishers: Dordrecht, The Netherlands, 2000.
(4) Glarborg, P.; Miller, J. A. *Combust. Flame* **1994**, *99*, 475.
(5) Smith, I. W. M. In *The Chemical Dynamics and Kinetics of Small Radicals*; Liu, K., Wagner, A., Eds.; World Scientific: Singapore, 1995; Part I.
(6) Becker, K. H.; Kurtenbach, R.; Schmidt, F.; Wiesen, P. *Combust. Flame* **2000**, *120*, 570.
(7) Schacke, H.; Schmatjko, K.; Wolfrum, J. *Arch. Procesow Spalania* **1974**, *5*, 363.
(8) Lifshitz, A.; Frenklach, M. *Int. J. Chem. Kinet.* **1980**, *12*, 159.
(9) Higashihara, T.; Kuoda, H.; Saito, K.; Murakami, I. *Combust. Flame* **1985**, *61*, 167.
(10) Louge, M.; Y.; Hanson, R. K. *Symp. (Int.) Combust., [Proc.]* **1985**, *20*, 665.
(11) Mertens, J. D.; Dean, A. J.; Hanson, R. K.; Bowman, C. T. *Symp. (Int.) Combust., [Proc.]* **1992**, *24*, 701.
(12) Mulvihill, J. N.; Phillips, L. F. *Symp. (Int.) Combust., [Proc.]* **1975**, *15*, 1113.
(13) Qu, Z.-W.; Zhu, H.; Li, Z.-S.; Zhang, X.-K. *Chem. Phys. Lett*. **2001**, *353*, 304.
(14) Rim, K. T.; Hershberger, J. F. *J. Phys. Chem. A* **1999**, *103*, 3721.
(15) Decker, B. K.; Macdonald, R. G., manuscript in preparation.
(16) He, G.; Tokue, I.; Harding, L.; Macdonald, R. G. *J. Phys. Chem. A* **1998**, *102*, 7653.
(17) Kroto, H. W. *Molecular Rotational Spectra*; Dover: New York, 1992.
(18) Decker, B. K.; Macdonald, R. G., manuscript in preparation.
(19) Knowels, P. J.; Werner, H.-J.; Hay, P. J.; Cartwright, D. C. *J. Chem. Phys.* **1988**, *89*, 7334.
(20) He, G.; Tokue, I.; Macdonald, R. G.; *J. Chem. Phys.* **1998**, *109*, 6312.
(21) Sablier, M. S.; Fujii, T. *Chem. Rev*. **2002**, *102*, 2855.
(22) Martin, J. M. L.; Taylor, P. R.; Francois, J. P.; Gijbels, R. *Chem. Phys. Lett*. **1994**, *226*, 475.
(23) Tsang, W. *J. Phys. Chem. Ref. Data* **1992**, *21*, 753.
(24) Titarchuk, T. A.; Halpern, J. A. *Chem. Phys. Lett*. **1995**, *232*, 192.
(25) Yang, D. L.; Lin, M. C. In *The Chemical Dynamics and Kinetics of Small Radicals*; Liu, K., Wagner, A., Eds.; World Scientific: Singapore, 1995; Part I.
(26) Brownsword, R. A.; Hancock, G.; Heard, D. E. *J. Chem. Soc., Faraday Trans*. **1997**, *93*, 2473.
(27) Becker, K. H.; Kurtenbach, R.; Schmidt, F.; Wiesen, P. *Ber. Bunsen-Ges. Phys. Chem.* **1997**, *101*, 128.
(28) Cooper, W. F.; Park, J.; Hershberger, J. F. *J. Phys. Chem.* **1993**, *97*, 3283.
(29) Wategaonkar, S.; Setser, D. W. *J. Phys. Chem.* **1993**, *97*, 10028.
(30) Gao, Y.; Decker, B. K.; Macdonald, R. G. Work in progress.
(31) Lee, J. H.; Michael, J. V.; Payne, W. A.; Stief, L. J. *J. Chem. Phys.* **1978**, *69*, 3069.
(32) Green, B. D.; Caledonia, G. E.; Murphy, R. E.; Robert, F. X. *J. Chem. Phys.* **1982**, *76*, 2441.
(33) Wysong, I. J. *J. Chem. Phys.* **1994**, *101*, 2800.
(34) Juang, D. Y.; Lee, J.-S.; Wang, N. S. *Int. J. Chem. Kinet.* **1995**, *27*, 1111.
(35) Atakan, B.; Wolfrum, J. *Chem. Phys. Lett.* **1991**, *178*, 157.
(36) Press, W. H.; Flannery, B. P.; Teukolsky, S. A.; Vetterling, W. T.; *Numerical Recipes*; Cambridge University Press: Cambridge, U.K., 1988; Chapter 15.
(37) Macdonald, R. G.; Sonnenfroh, D. M.; Liu, D.-J.; Liu, K. *Can. J. Chem.* **1994**, *72*, 660.
(38) Philips, L. F.; Smith, I. W. M.; Tukett, R. P.; Whitham, C. J. *Chem. Phys. Lett.* **1991**, *183*, 254.
(39) Sauder, D. G.; Dipti, P.-M.; Dagdigian, P. J. *J. Chem. Phys.* **1991**, *95*, 1696.
(40) Hancock, G.; McKendrick, K. G. *Chem. Phys. Lett.* **1986**, *127*, 125.
(41) Astbury, C. J.; Hancock, G.; McKendrick, K. G. *J. Chem. Soc., Faraday Trans.* **1993**, *89*, 405.
(42) Fernandez, J. A.; Husain, D.; Sanchez Rayo, M. N.; Castano, F. *J. Chem. Phys.* **1997**, *106*, 7090.
(43) Macdonald, R. G.; Liu, K. *J. Chem. Phys.* **1993**, *98*, 3716.
(44) Lin, M. C.; He, Y.; Melius, C. F. *J. Phys. Chem*. **1993**, *97*, 9124.
(45) Holbrook, R. *Unimolecular Reactions*; Wiley-Interscience: London, 1972.
(46) Balla, R. J.; Pasternack, L. *J. Phys. Chem.* **1987**, *91*, 73.
(47) North, S. W.; Hall, G. E. *J. Chem. Phys.* **1997**, *106*, 60.
(48) Pine, A. S.; Maki, A. G.; Chou, N.-Y. *J. Mol. Spectrosc.* **1985**, *114*, 132.
(49) Devi, V. M.; Benner, D. C.; Rinsland, C. P.; Smith, M. A. H. *J. Quant. Spectrosc. Radiat. Transfer* **1998**, *60*, 741.
(50) Mohammad, F.; Morris, V. R.; Fink, W. H.; Jackson, W. M. *J. Phys. Chem*. **1993**, *97*, 11590.
(51) Vallance, C.; Maclagan, R. G. A. R.; Phillips, L. F. *Chem. Phys. Lett.* **1996**, *250*, 59.
(52) Tully, J. C. *J. Chem. Phys.* **1971**, *62*, 1893.
(53) Phillips, L. F. *J. Phys. Chem. A* **1998**, *102*, 31.
(54) Graff, M. M.; Wagner, A. F. *J. Chem. Phys.* **1990**, *92*, 2423.
(55) Takayanagi, T.; Kurosaki, Y.; Sato, K.; Misawa, K.; Kobayashi, Y.; Tsunashima, S. *J. Phys. Chem. A* **1999**, *103*, 250.
(56) Macy, T. P.; Diaz, R. R.; Heard, D.; Leone, S. R.; Harding, L. B.; Klippenstein, S. J. *J. Phys. Chem. A* **2001**, *105*, 8361.